Supplement for:
Impact of stratospheric air and surface emissions on tropospheric nitrous oxide during ATom

Gonzalez et al.

Table of Contents

S1. Latitudinal variability of tropospheric N_2O during ATom……2
S2. Surface N_2O from the NOAA-MBL flask sampling network ……2
S3. Supporting Figures and Tables……..3
S4. References……..15

S1. Latitudinal variability of tropospheric N_2O during ATom

Altitudinal, latitudinal, and seasonal distributions of N_2O during ATom are shown in Figure S5. Overall, depleted N_2O is mainly observed at high latitudes (> 60°) in upper troposphere/lower stratosphere (UT/LS, 8 – 12.5 km, Figures S–5 and S–6(a–b), where it ranged between 281 and 333 ppb (Table S.3). In the northern high latitudes (NHL), the 10-s measurements of N_2O ranged between 281 and 333 ppb in the Pacific basin, and between 297 and 330 ppb in the Atlantic. In the southern high latitudes (SHL), N_2O ranged between 307 and 331 ppb in the Pacific basin, and between 297 and 330 ppb in the Atlantic. At middle latitudes (ML, 30° – 60°), N_2O mixing ratios ranged between 301 and 335 ppb in the Northern Hemisphere (NH) and between 297 and 335 ppb in the Southern Hemisphere (SH, see Table S.3). Close to the equator (30° S – 30° N, 319 to 336 ppb) we found the highest mixing ratios of N_2O.

The latitudinal distribution of N_2O in the free troposphere (FT, 2 – 8 km) and in the marine boundary layer (MBL, < 2km) are very similar where mean values are compared (Table S.3). In the troposphere (below < 8 km), N_2O mixing ratios slightly increase towards northern latitudes as a result of higher anthropogenic emissions in the Northern Hemisphere relative to the Southern Hemisphere (Figures S6(c-f)). The gradient between the equator and high NH latitudes is quite small as a result of the location of the surface maximum, which is sometimes near the equator and sometimes in the NH mid or high latitudes. The mean distributions of N_2O are also very similar between oceans. Small differences are mainly caused by the influence of continental polluted airmasses transported from the continents over the oceans.

S2. Surface N_2O from the NOAA-MBL flask sampling network

We use the weekly N_2O air samples from the NOAA Greenhouse Gas Marine Boundary Layer Reference from the NOAA GMD Carbon Cycle Group (NOAA/ESRL GMD CCGG, https://www.esrl.noaa.gov/gmd/ccgg/mbl/), hereafter NOAA-MBL, to constrain a latitudinal gradient of N_2O mixing ratios (MRs) at the surface for each ATom deployment.

The time series of the latitudinal gradient of N_2O based on NOAA-MBL flask samples from the period 2000 to 2020 is shown in Figure S7. This figure emphasizes the annual increasing trend of N_2O (0.9 ppb per year) and the higher N_2O MRs in the NH relative to the SH. The detrended series highlights a surface N_2O minimum between April and June in the SH and between July and September in the NH (Figures S8 and S9). This N_2O minimum is caused by the downward propagation of stratospheric air during the polar vortex break-up (between November–December in the SH and March–April in the NH), reaching the surface with a 3-month delay (Nevison et al., 2011 and references therein). The surface impact of this downward propagation of air depleted in N_2O is clearly observed in the SH during May (AT-4, Figure S10).

S3.Supporting Figures and Tables

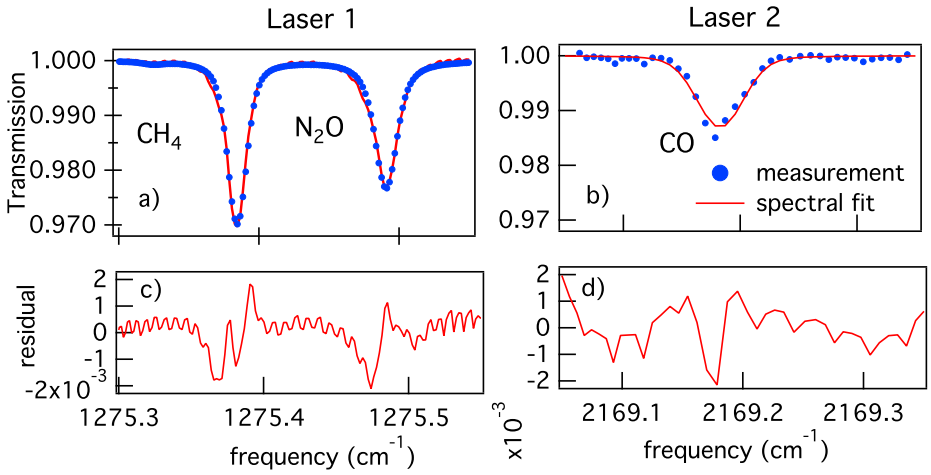

Figure S1. Spectra and fit residual for CH_4, N_2O and CO measured during the in-flight injection of the high mixing ratio gas cylinder (2182.5, 339.1, and 192.9 ppb for CH_4, N_2O, and CO respectively). The optical path length is 76 m. During flight, the cell is held at a constant pressure of 58.3 Torr. The fraction of absorption of these lines were 2.7 % for CH_4, 2.1% for N_2O and 1.4 % for CO. (a) Laser 1 spectrum that targets CH_4 and N_2O and (b) laser 2 spectrum targeting CO. In the top plots, measurements are blue dots and the spectral fit is as a red line. The lower plots represent the residual (difference between measured and fit transmission spectra) for (c) laser 1 and (d) laser 2.

Figure S2. Example of sampling sequence measured during ATom for (a) CH_4, (b) N_2O, and (c) CO. Calibrations include 2 minutes of zero air (Z) followed by 1 minute of low (LS) and high (HS) mixing ratio gas standards, repeated every 30 minutes.

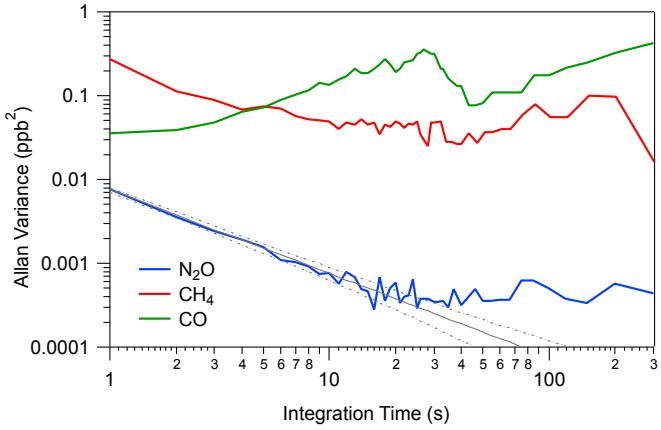

Figure S3. Allan-Werle variance analysis obtained during an ATom-2 flight segment above the remote Pacific Ocean. The analysis showed 1 s standard deviations of 0.5, 0.09, and 0.19 ppb for CH_4, N_2O, and CO, respectively.

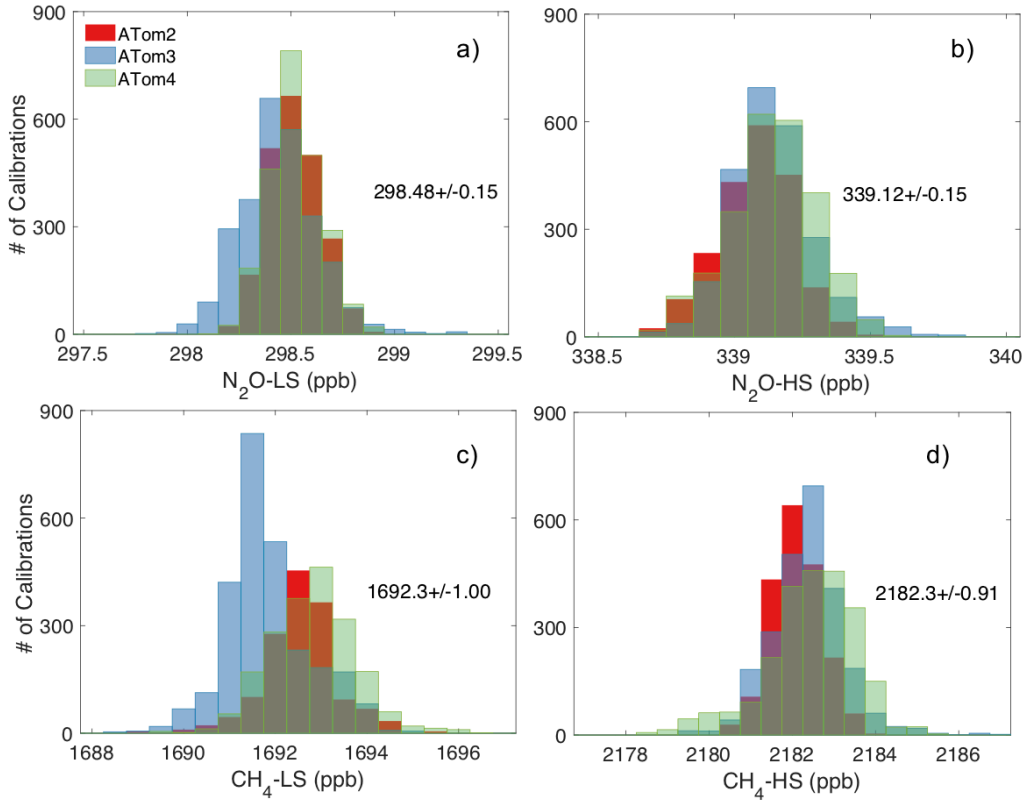

Figure S4. Distribution of 1-minute average calibration data for (a) N_2O low span (N_2O-LS), (b) N_2O high span (N_2O-HS), (c) CH_4-LS and (d) CH_4-HS, separated by mission. ATom-2 is shown in red, ATom-3 in blue and ATom-4 in green, after the application of the PCA. In each plot, the corresponding mean and standard deviation of the 3 missions combined is shown. The standard deviation of the calibrations during the mission was 0.2 ppb for N_2O and 1 ppb for CH_4.

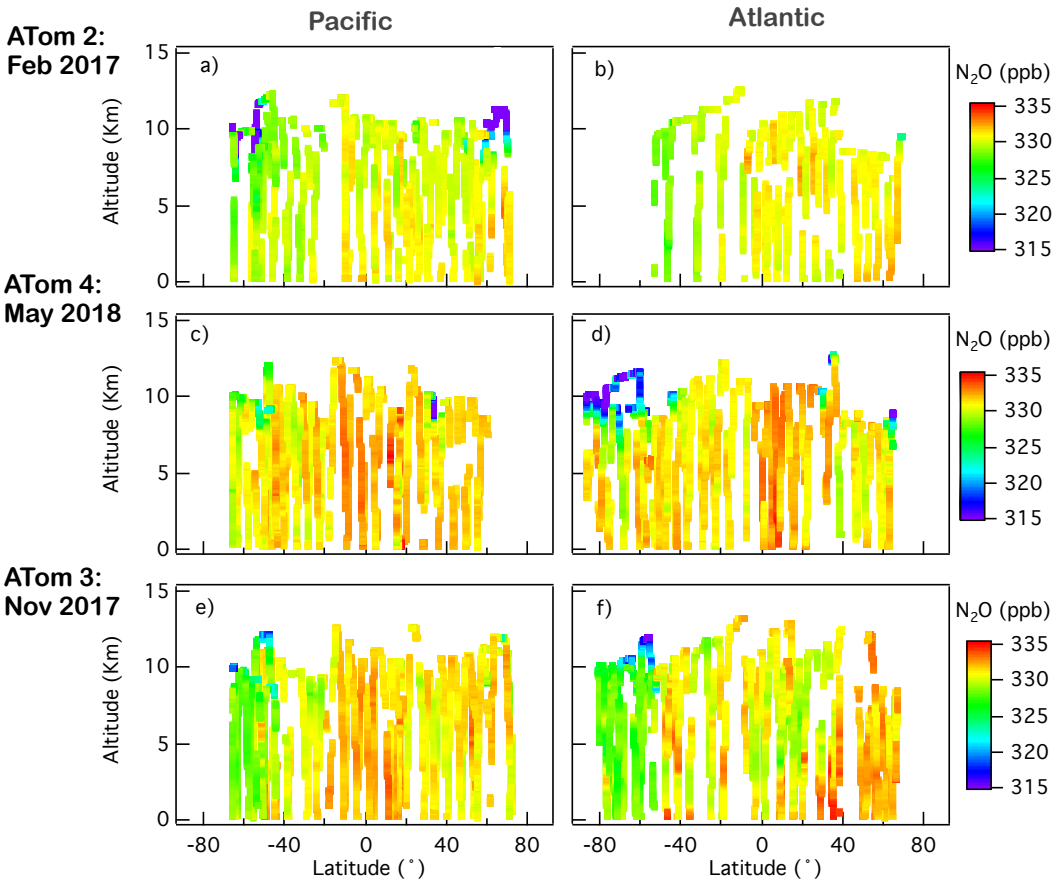

Figure S5. Altitudinal, latitudinal, and seasonal distributions of QCLS N_2O observed during ATom-2, -3, and -4. Each row represents each deployment organized top to bottom by season. The left column are profiles measured in the Pacific and right column are right column are those in the Atlantic. The data are colored by N_2O mixing ratios between 315 to 335 ppb, with values outside this range shown in the same extreme color (violet for values < 315 ppb and red for values > 335 ppb).

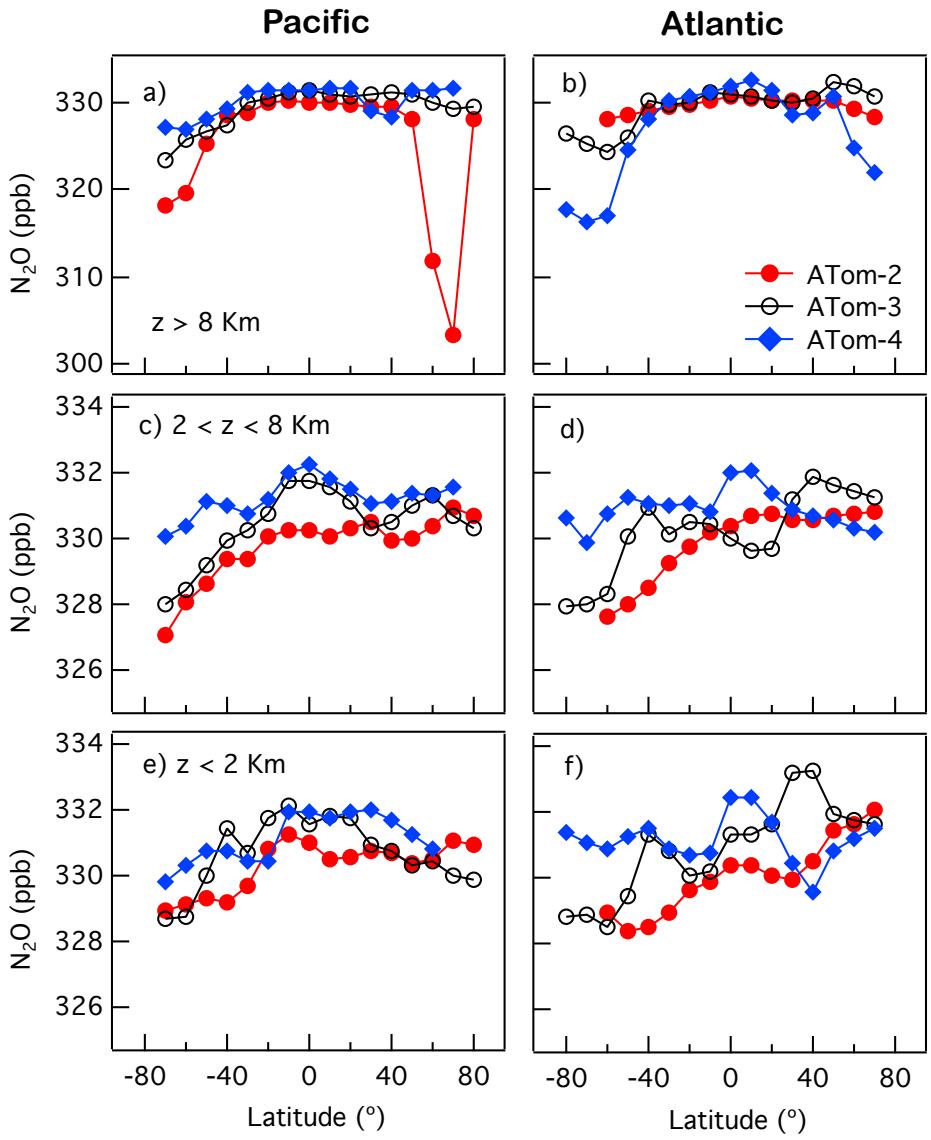

Figure S6. Latitude-binned mean N_2O mixing ratios observed within 10° latitude bands (a)-(b) in the upper troposphere/lower stratosphere (UTLS, 8 – 12.5 km), (c)-(d) in the free troposphere (2 - 8 km) and (e)-(f) in the MBL (< 2 km) during ATom-2 (red circles), ATom-3 (black open circles), and ATom-4 (blue diamonds).

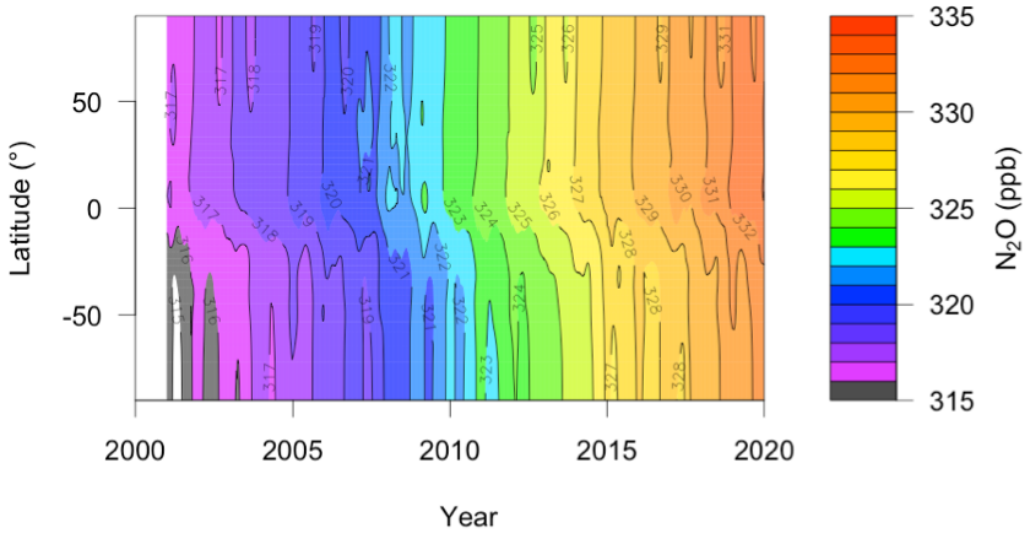

Figure S7. Time series of the latitudinal gradient of N_2O mixing ratios based on NOAA-MBL product based on flask samples from surface sites (period 2000 to 2020).

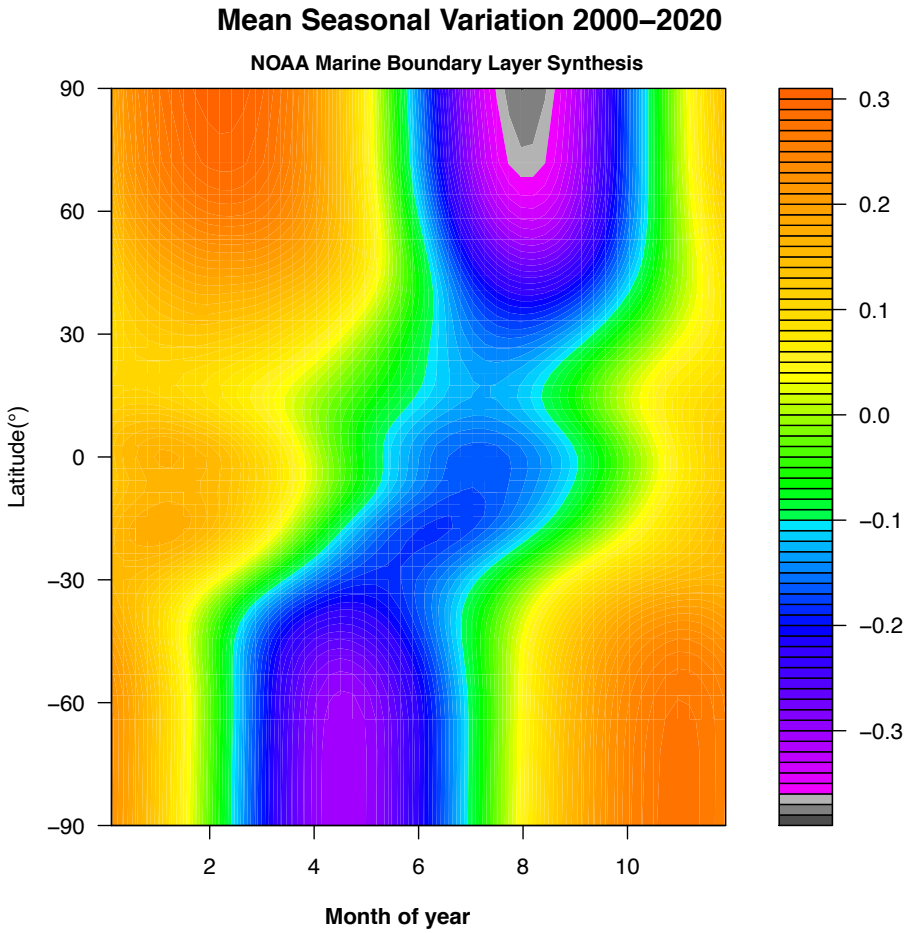

Figure S8. Cross-section of detrended monthly mean of the tropospheric N_2O background based on NOAA-MBL flask samples from the period 2000 to 2020.

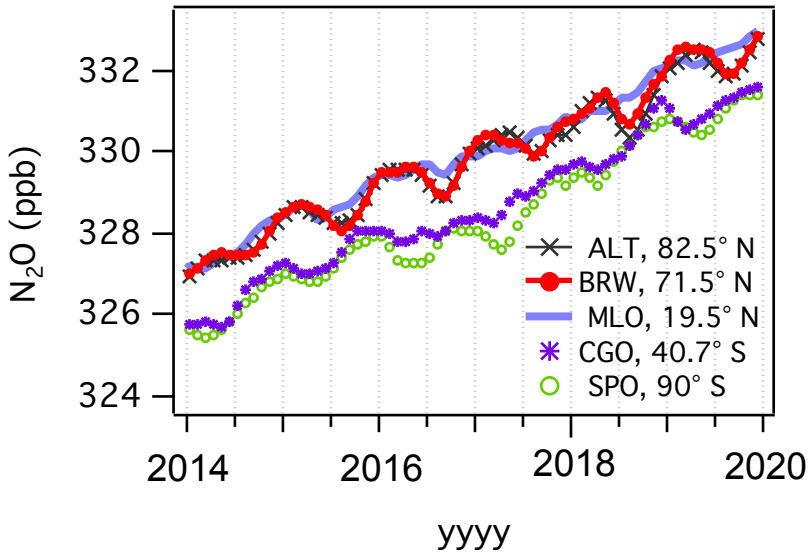

Figure S9. Seasonal variations and trends of N_2O at remote Pacific surface stations. Seasonal minima occur in August-September in the Northern Hemisphere, and in March-April in the Southern Hemisphere, 2–4 months after breakup of the polar vortices in spring.

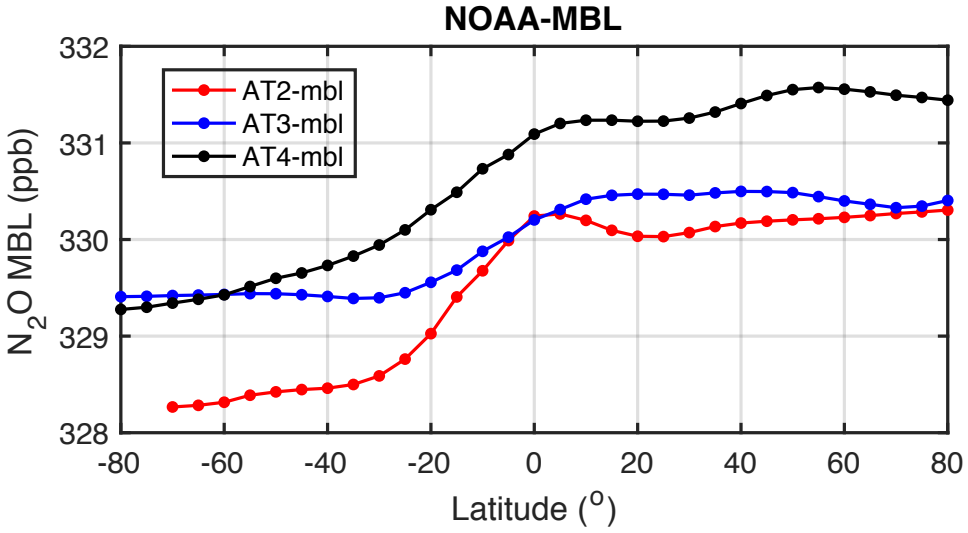

Figure S10. Latitudinal gradient of N_2O mixing ratios from the NOAA-MBL product of flask samples collected at surface stations for AT-2, -3 and -4.

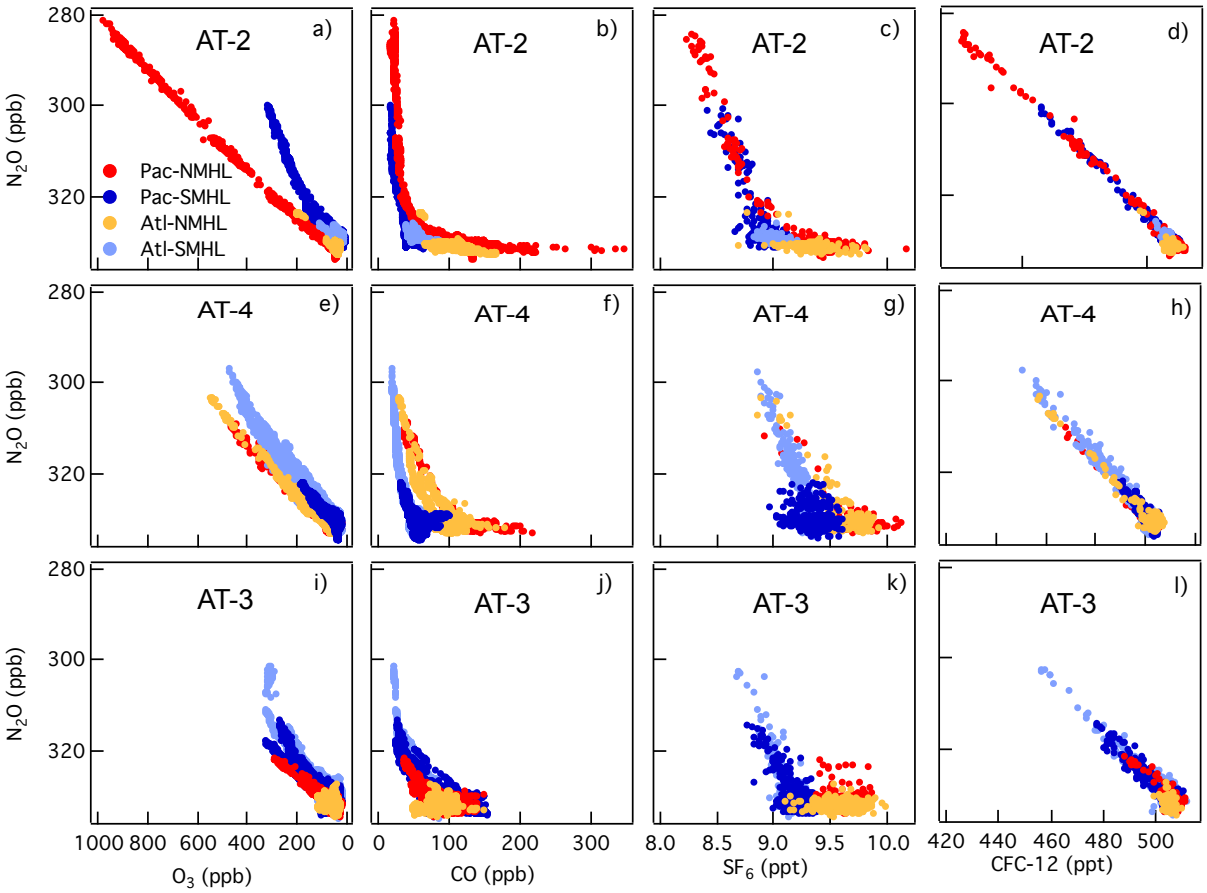

Figure S11. Tracer-tracer correlations between N_2O, O_3, CO, SF_6 and CFC-12 at middle and high latitudes (30° - 85°). The data are organized from top to bottom by months of the year: ATom-2 (a – d), ATom-4 (e – h) and ATom-3 (i – l). The data are colored as a function of the ocean basin and hemisphere: Pacific North Mid-High Latitudes (Pac-NMHL, >30°N) in red, Pacific South Mid-High Latitudes (Pac-SMHL, <30°S) in dark blue, Atlantic South Mid-High Latitudes (Atl-SMHL, <30°S) in light blue and North Mid-High Latitudes (Atl-NMHL, >30°N) in orange. Note that the N_2O and O_3 axes are reversed.

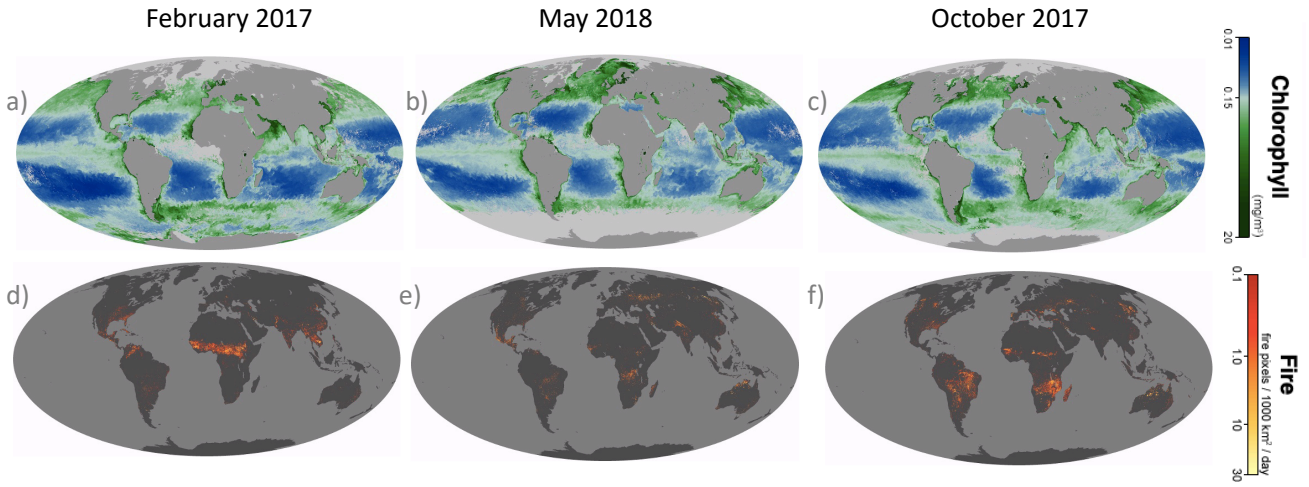

Figure S12. Global maps of monthly mean Moderate Resolution Imaging Spectroradiometer (MODIS) of chlorophyll (mg/m^3) and fire pixels (1000 km^2 /day) from the NASA Earth Observatory (https://earthobservatory.nasa.gov/global-maps). Plots are shown from left to right by season.

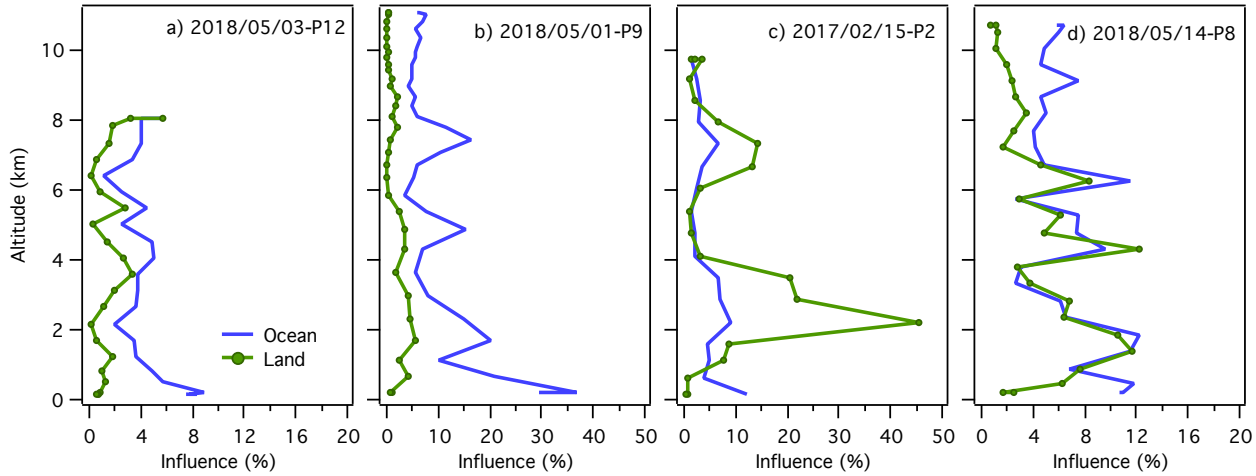

Figure S13. Surface influence coming from the land and ocean for the profiles shown in the manuscript (Figures 5 to 8) based on the analysis of backtrajectories.

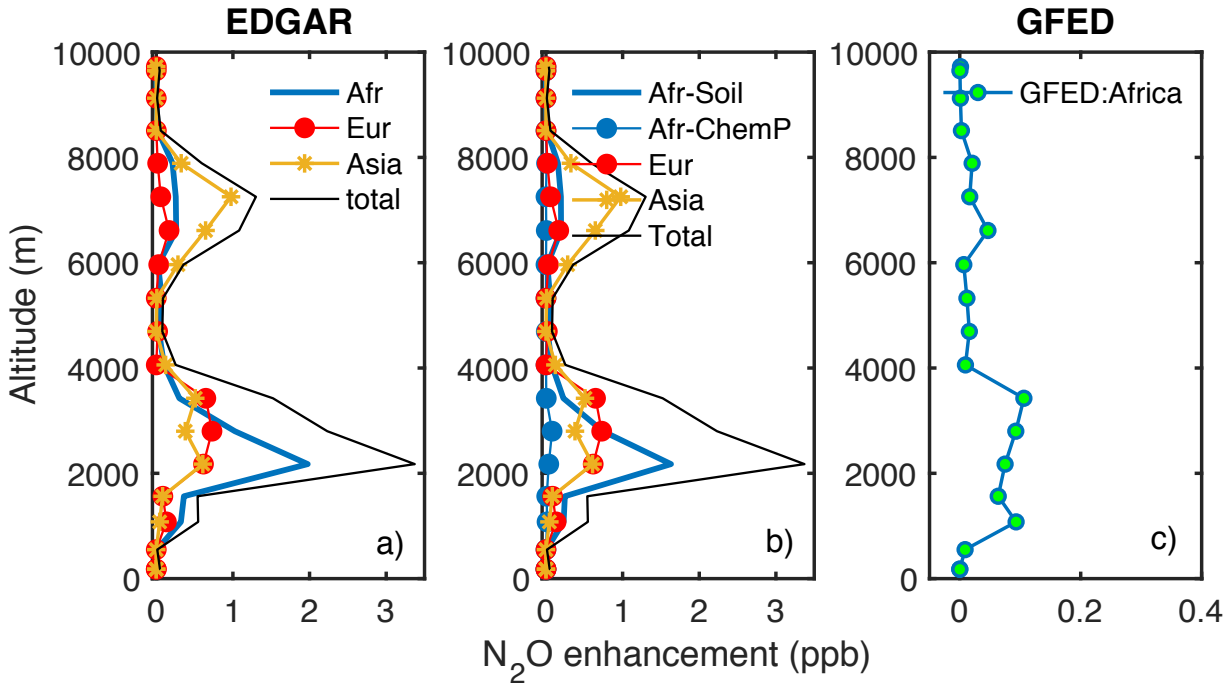

Figure S14. N_2O mean enhancement estimated by the inventories databases EDGAR (a-b) and GFED (c) for February 2017. Plot (a) shows the total N_2O contributions from EDGAR inventory for Africa (blue), Europe (red) Asia (yellow) and global (black). In plot (b) shown the N_2O contribution from Africa has been split into soil / agriculture and chemical processes contributions. EDGAR suggests major contribution to the observed N_2O enhancements to emission from agriculture and industrial chemical processes. Plot (c) shows the relatively small N_2O contribution from biomass burning emissions from Africa provided by GFED. Note that the smaller scale in the x-axis of the GFED enhancements (c).

Table S.1. Calibration dates and mixing ratios of the primary cylinders used during ATom. These cylinders were calibrated at NOAA using the WMO – NOAA primary standards WMO X2004A for CH_4, WMO X2014A for CO and NOAA-2006A for N_2O. Two methods were used in the CO calibration; [1]off-axis integrated cavity output spectroscopy (OA-ICOS) and [2]vacuum ultraviolet resonance fluorescence spectroscopy (VURF). NOAA ESRL cylinder calibration laboratory note that the VURF results are typically ~0.5 to 1.5 ppb lower than the OA-ICOS results over the range 50 - 500 ppb CO.

Cylinder ID	Cal Date	CH_4	N_2O	CO
			mean ± 1σ (ppb)	
CB11484	2018-08-20		339.09 ± 0.13	
	2018-07-25			192.87 ± 0.37[2]
	2018-07-25			193.40 ± 0.04[1]
	2018-07-10			193.03 ± 0.29[2]
	2018-07-10			193.09 ± 0.06[1]
	2018-06-18			192.48 ± 0.60[2]
	2018-06-18			193.14 ± 0.04[1]
	2018-06-18	2182.52 ± 0.17		
	2018-06-15	2182.61 ± 0.16		

	2017-04-21		339.14 ± 0.13		
	2017-03-20			191.68 ± 0.07[1]	
	2017-03-17	2182.87 ± 0.66			
	2015-10-22			189.62 ± 0.11[1]	
	2015-10-16			189.60 ± 0.08[1]	
	2015-10-14			189.30 ± 0.10[1]	
	2015-10-05		339.08 ± 0.13		
	2015-09-28	2182.34 ± 0.82			
	2015-09-21	2182.09 ± 0.76			
	2015-09-15	2182.46 ± 0.62			
CB10182	2018-08-08		298.51 ± 0.07		
	2018-07-25			118.76 ± 0.11[2]	
	2018-07-25			119.38 ± 0.03[1]	
	2018-07-10			119.29 ± 0.28[2]	
	2018-07-10			119.29 ± 0.02[1]	
	2018-06-28	1692.37 ± 0.10			
	2018-06-19			118.60 ± 0.27[2]	
	2018-06-19			119.33 ± 0.02[1]	
	2018-06-15	1692.34 ± 0.09			
	2017-05-04		298.53 ± 0.15		
	2017-03-21			117.94 ± 0.04[1]	
	2017-03-17	1692.40 ± 0.46			
	2015-10-22			116.68 ± 0.03[1]	
	2015-10-13	1692.61 ± 0.73		116.78 ± 0.07[1]	
	2015-10-07	1692.30 ± 0.63			
	2015-10-06			116.81 ± 0.09[1]	
	2015-09-24		298.47 ± 0.09		

Table S.2. Fit parameters for the comparisons between QCLS and the other three instruments measuring N_2O on board (PANTHER, UCATS and PFP, respectively) in each ATom deployment (-2, -3 and -4). The 95% C.I. of the difference (95% C.I.) between QCLS and the other instruments is also included.

Mission	QCLS vs PANTHER		QCLS vs UCATS		QCLS vs PFP	
	s, i[a]	*95% C.I.*	*s, i*	*95% C.I.*	*s, i*	*95% C.I.*
ATom 2	0.92, 26.91	-0.27 ± 0.47	0.94, 19.56	1.20 ± 0.05	0.96, 14.08	1.03 ± 0.13
ATom 3	0.91, 31.36	1.34 ± 0.06	0.75, 83.04	1.66 ± 0.08	0.84, 54.80	1.49 ± 0.19
ATom 4	0.98, 6.16	0.90 ± 0.06	0.97, 9.66	0.78 ± 0.05	0.92, 26.28	1.18 ± 0.18

[a]Slope (s) and intercept (i) for a linear fit of the correlation plot for each pair of instruments.

Table S.3. Median N_2O mixing ratios observed at different latitudinal regions and altitude sectors during ATom-2, -3 and -4.

Ocean	Mission	Altitude	SHL[a]	SML[b]	Equator[c]	NML[d]	NHL[e]
	ATom-2	< 2 km	-	328.53	330.15	331.25	332.23
		2 – 8 km	-	328.62	330.48	330.54	330.97
		> 8 km	-	328.82	330.07	330.20	329.79

Atlantic	ATom-3	< 2 km	328.86	329.55	331.28	332.18	331.61
		2 – 8 km	328.06	330.13	329.80	331.64	330.99
		> 8 km	326.23	329.55	330.56	330.88	330.98
	ATom-4	< 2 km	331.27	331.23	331.55	330.28	331.45
		2 – 8 km	330.74	331.19	331.50	330.73	330.71
		> 8 km	317.59	329.95	331.77	330.91	326.50
Pacific	ATom-2	< 2 km	328.94	329.04	330.77	330.60	331.06
		2 – 8 km	327.59	329.02	330.35	330.03	330.79
		> 8 km	314.01	328.50	329.98	329.74	307.71
	ATom-3	< 2 km	328.78	330.08	331.57	330.48	329.85
		2 – 8 km	328.03	329.35	331.28	330.86	330.75
		> 8 km	324.35	328.22	331.07	331.06	329.86
	ATom-4	< 2 km	329.80	330.75	331.88	330.52	-
		2 – 8 km	330.29	331.03	331.72	331.28	331.57
		> 8 km	327.14	329.76	331.38	331.20	331.66

[a]SHL (< 60° S)
[b]SML (60° S - 30° S)
[c]Equator (30° S - 30° N)
[d]NML (30° N - 60° N)
[e]NHL (>60° N)

S4.References

Nevison, C. D., Dlugokencky, E., Dutton, G., Elkins, J. W., Fraser, P., Hall, B., Krummel, P. B., Langenfelds, R. L., O'Doherty, S, Prinn, R. G., Steele, L. P., and Weiss, R. F.: Exploring causes of interannual variability in the seasonal cycles of tropospheric nitrous oxide, Atmos. Chem. Phys., 11, 3713–3730, doi:10.5194/acp-11-3713-2011, 2011.